EFFECT OF HEAVY METALS ON DYNAMIC AND STATIC QUENCHING OF THE FLUORESCENCE OF THE HOST-GUEST INCLUSION COMPLEX METHYL-β-CYCLODEXTRIN BY 2,9-DIMETHYL-4,7-DIPHENYL-1,10-PHENANTHROLINE IN AQUEOUS MEDIA**

Umit Ay

Department of Chemistry, Kocaeli University, 41380, Kocaeli, Turkey;
e-mail: *umurege@kocaeli.edu.tr, umitay36@hotmail.com*

An inclusion complex was formed with methyl-β-cyclodextrin (Me-β-CD) and the smallest unit of the macrocyclic family of bathocuproine[Ed1], 2,9-dimethyl-4,7-diphenyl-1,10-phenanthroline. With this newly formed fluorescent probe, the quenching effect of heavy metals was investigated. Spectral characterization of the complex was performed by UV-visible and fluorescence spectroscopy techniques. The complex formation constant (K_b), Gibbs free energy (ΔG^0) and approximate quenching activation energy (E_a) values were calculated. Lifetime (τ), bimolecular quenching rate constant (k_q) values, and diffusion rate constant (k_d) calculations were made, and the mechanism of quenching by the effect of heavy metals was clarified.

Keywords: *inclusion complex, transition metals, quenching mechanism, fluorescence lifetime, bathocuproine.*

ВЛИЯНИЕ ТЯЖЕЛЫХ МЕТАЛЛОВ НА ДИНАМИЧЕСКОЕ И СТАТИЧЕСКОЕ ТУШЕНИЕ ФЛУОРЕСЦЕНЦИИ МЕТИЛ-β-ЦИКЛОДЕКСТРИНА 2,9-ДИМЕТИЛ-4,7-ДИФЕНИЛ-1,10-ФЕНАНТРОЛИНОМ В ВОДНЫХ СРЕДАХ

U. Ay

УДК 535.372

Университет Коджаэли, Коджаэли, 41380, Турция;
e-mail: *umurege@kocaeli.edu.tr, umitay36@hotmail.com*

(Поступила 12 февраля 2020)

Комплекс включения образован метил-β-циклодекстрином (Me-β-CD) и наименьшей единицей макроциклического семейства батокупроина — 2,9-диметил-4,7-дифенил-1,10-фенантролином. С помощью этого флуоресцентного зонда исследован эффект тушения флуоресценции тяжелых металлов. Комплекс охарактеризован методами УФ-видимой и флуоресцентной спектроскопии. Рассчитаны комплексная константа (K_b), свободная энергия Гиббса (ΔG^0), энергия активации тушения (E_a), время жизни (τ), константа скорости бимолекулярной закалки (k_q) и константа скорости диффузии (k_d), а также уточнен механизм тушения под действием тяжелых металлов.

Ключевые слова: *комплекс включения, переходные металлы, механизм тушения, время жизни флуоресценции, батокупроин.*

Introduction. Many bathocuproine (BCP) derivatives have been synthesized as candidates for exciton blocking layers (EBLs) in organic solar cells and investigated [1]. In addition, many studies have reported that 2,9-dimethyl-4,7-diphenyl-1,10-phenanthroline (bathocuproine) is a promising hole blocking material for the production of high-performance OLEDs[Ed2] [2–4]. Bathocuproine is also used as a suitable activator to strengthen the catalytic effect of specific metal ions in the determination of trace levels of copper(II) and iron(III) [5]. Cyclodextrins (CDs) are macrocyclic ring-shaped molecules formed by D(+)-

**Full text is published in JAS V. 88, No. 4 (http://springer.com/journal/10812) and in electronic version of ZhPS V. 88, No. 4 (http://www.elibrary.ru/title_about.asp?id=7318; sales@elibrary.ru).

glucopyranose units. CDs are suitable for forming supramolecular assemblies via the formation of an inclusion complex with low-molecular-weight compounds and polymers. The size, shape, and polarity of the guest molecule, with relatively low polar internal activity compared to CDs, are important parameters for complexation. β-CDs are the best natural hosts in the CD family and are known as small organic molecules. β-CD has a depth of 0.8 nm and a diameter of 0.7 nm [6]. The inclusion complex formed with CD is fluorescent and generally yields a high fluorescence quantum yield. Hydrogen bonds between the cyclodextrin cavity and the hydrophobic particles of the guest molecule and van der Waals interactions/hydrophobic interactions between the cyclodextrin hydroxyl groups and the polar functional groups of the guest molecule are considered to be the forces related to the high-energy water molecules released from the cavities in the complex formation process and to the stress energy activated in CD system formation [Ed3][7]. For the first time, in this study, an inclusion complex was formed by combining these two compounds, and the subsequent quenching mechanism of Fe^{2+}, Fe^{3+}, and Ni^{2+} was investigated.

We synthesized a novel inclusion complex of Me-β-CD and BCP, which, to the best of our knowledge, has not been reported elsewhere. We believe that this work represents an initial step to investigate the feasibility of the interaction of Me-β-CD and BCP. Thus, we chose simple, highly sensitive and selective methods, such as UV-visible and fluorescence spectroscopy, for the characterization of inclusion complexes. After the characterization study, the change in the intensity of fluorescence emission caused by the heavy metal effect was examined. Using Benesi-Hildebrand's method, the stoichiometry of BCP-Me-β-CD host-quest complexes was obtained. Stern-Volmer (S-V) quenching constants were calculated from the slope of S-V plots (plots I_0/I to [Me-β-CD]). Fluorescence quantum yields (ϕ_F), bimolecular quenching rate constants, and approximate activation energy values were calculated for the BCP-Me-β-CD complex. In addition, different parameters for the quenching processes were determined using the sphere-of-action static quenching model and the finite sink approximation model, and the quenching mechanism was elucidated. The effect of metal ions on the quenching mechanism was observed.

Materials and methods. Me-β-CD (mean molecular weight 1310 g/mol; Aldrich, Steinheim, Germany), bathocuproine, and chloroform (Merck, Darmstadt, Germany) were used in this study. For fluorescence lifetime measurement, Ludox-AS-30 colloidal silica (Sigma-Aldrich Chemie Gmbh) was used as the reference solution. All solutions of metal ions were prepared from analytical-grade nitrate and chlorine salts (Merck, Darmstadt) and were dissolved in double-distilled water. All other chemicals were of analytical reagent grade and were used as received without further purification.

Host-guest inclusion complexes were prepared by dissolving BCP at concentrations ranging from 10^{-3} to 10^{-5} M with 10^{-3} M Me-β-CD in 100 mL of purified water. The solutions were stirred at room temperature with a magnetic stirrer for 24 h. The effect of mixing time on inclusion complex formation was clearly seen in our previous studies with anthracene and naphthalene [7, 8]. A mixing time of less than 24 h affects the quantum yield and the complex formation constant. No effect was observed in the case of mixing for more than 24 h. Therefore, in this study, 24 h was selected for inclusion complex formation. Finally, the solution was transferred to volumetric containers. Complex formation in solution is a dynamic equilibrium process. The reaction is as follows:

$$\text{BCP} + \text{Me-β-CD} \leftrightarrow \text{BCP-Me-β-CD}. \quad (1)$$

First, fluorescence measurements of the prepared inclusion complexes in 1.0×1.0 cm^2 quartz cells were made. The effect of metal ions on fluorescence spectra was investigated by directly adding metal ions from stock solutions at the microliter level through micropipettes to inclusion complexes of known volume (1.5 mL). Emission spectra were recorded at an excitation wavelength of 300 nm. Fluorescence measurements were made using a Varian Agilent Cary Eclipse [Ed4]instrument with 1×1 cm^2 quartz cells. A PG Instrument T70+ model spectrophotometer was used for the measurement of absorption spectra. Fluorescence lifetimes were measured using a time-correlated single-photon counting setup (TCSPC) (Horiba Fluorolog 3). Signal acquisition was performed using a TCSPC module (NanoLED, emission at 390 nm).

Results and discussion. *Fluorescence spectroscopy.* Since Fe^{2+}, Fe^{3+}, and Ni^{2+} metal cations do not have fluorescence properties, the quenching effect of these three metal ions on the inclusion complex was investigated by BCP. A probe molecule was successfully prepared. The volume of the outer sphere of Me-beta-CD is 773.18 $Å^3$, and the cavity volume is approximately 262 $Å^3$. The volume of the BCP molecule is approximately 672 $Å^3$. This shows that the BCP molecule cannot fully enter Me-β-CD. There is a partial interaction here. In addition, dimer, aggregate, and micelle formation may occur instead of inclusion complex formation in aqueous medium. Micellar formation at high temperature with supramolecular interactions for

surfactants is quite favorable. As the temperature decreases, cyclodextrins consist of surfactant monomers and unstable micelle complexes. Micelles usually occur in water, and the hydrophobic effect is the main driving force. Due to the formation of electrostatic repulsion between hydrophilic groups, surfactant molecules are separated and arranged loosely. This causes the formation of aggregates of greater size in ionic liquids than in aqueous systems. There are two types of aggregates formed. According to the aggregate formed, the absorption band may show a bathochromic shift. This aggregate is called the J-aggregate. If the blueshifted band is observed, the aggregate is called an H-aggregate. High quantum efficiency is observed in J-aggregates, while low quantum efficiency is observed in H-aggregates [9]. In this study, aggregate formation was studied at 25°C. In other words, neither high nor low temperatures were studied. The aggregation of BCP was prevented by inclusion complex formation. Complex formation was studied by UV-visible and fluorescence spectroscopy. The inclusion complex was formed by retaining BCP in the hydrophobic cavity of Me-beta-CD. In this way, aggregation of BCP was prevented. The stoichiometry of the complex formed using the Benesi-Hildebrand method has been shown to be 1:1 [8]. This method was not used due to the low coefficient of determination of the graph showing the 2:1 stoichiometric ratio of complex formation. From the slope of the graph obtained with Me-β-CD concentrations ranging from 1×10^{-2} to 1×10^{-5} M, the K_b binding constant was found to be 2×10^5 M^{-1} (Fig. 1). The magnitude of this value indicates strong inclusion complex formation. Using this value, the Gibbs free energy value (ΔG^0) [10] was calculated as –30 kJ/mol at room temperature. The negative value of ΔG^0 suggests that the inclusion process proceeded spontaneously at 298.15 K. From the wavelength at the point where the bathocuproine excitation and emission spectra overlapped, the excited singlet state energy was calculated to be 315 kJ/mol. This value usually ranges from 200 to 600 kJ/mol [8].

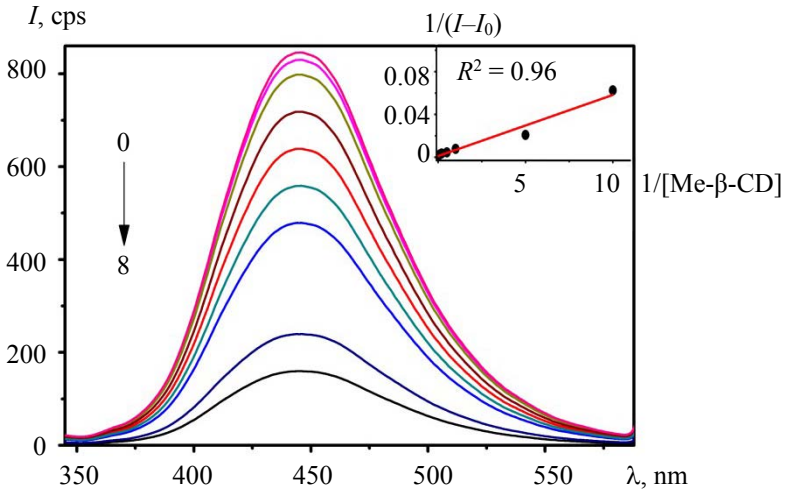

Fig. 1. The effect of increasing methyl-β-cyclodextrin concentration on the fluorescence spectrum of bathocuproine (1×10^{-5} M) dissolved in chloroform. Benesi-Hildebrand graph ($1/(I - I_0)$ vs 1/[Me-β-CD]) (insert). [BCP] = 1×10^{-5} (0), 1×10^{-2} (1), 5×10^{-3} (2), 1×10^{-3} (3), 5×10^{-4} (4), 2×10^{-4} (5), 1×10^{-4} (6), 2×10^{-5} (7), and 1×10^{-5} M (8); λ_{exc} = 300 nm.

Figure [Ed5]2 show the change in fluorescence intensities when the BCP concentration of Fe^{2+}, Fe^{3+}, and Ni^{2+} metal ions were between 10^{-3} and 10^{-5} M. The experimental results for the metals are shown in Fig. 2. In addition, in some of the graphs for the metals, some decomposition was observed in the characteristic emission spectrum of bathocuproine. Therefore, it was difficult to calculate a statistically valid K_{sv} value for these concentrations. The K_{sv} graphs for the metals are given in Fig. 3. To understand the quenching mechanisms, the Stern-Volmer was implemented for the steady state [11]:

$$I_0/I = 1 + K_{sv}[Q], \quad (2)$$

where K_{sv} was obtained from the linear fit line.

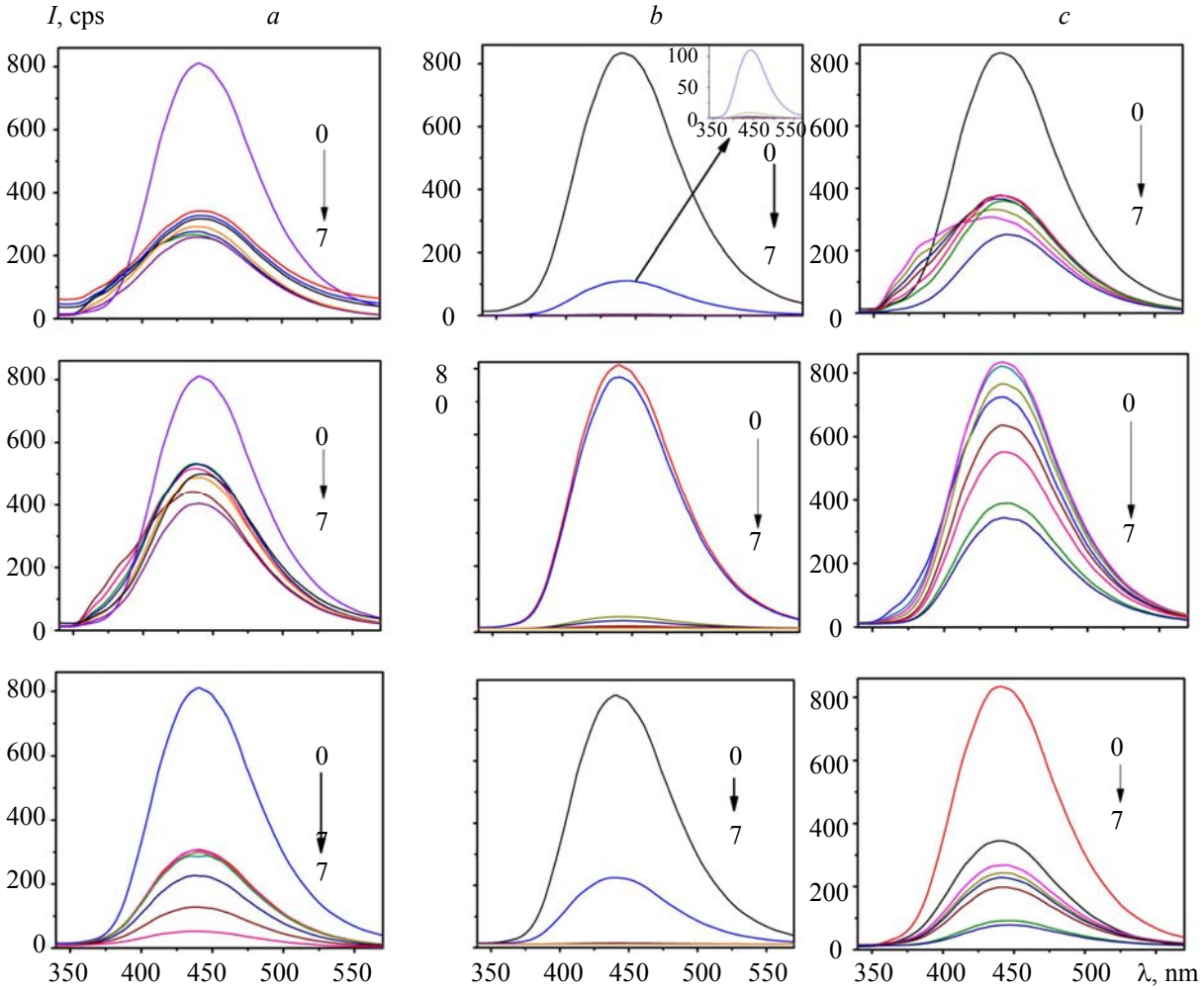

Fig. 2. Quenching effect on (a) BCP of 0.1 M Fe^{2+}, (b) BCP of 0.1 M Fe^{3+}, and (c) BCP of 0.1 M Ni^{2+}, in aqueous solution ([Me-β-CD] = 10^{-3} M). [BCP] = 10^{-3}, 10^{-4}, and 10^{-5} M (0); 0.23 (1), 0.33 (2), 0.67 (3), 1.66 (4), 3.33 (5), 6.67 (6), and 10.00 mM (7) Fe^{2+} (a), Fe^{3+} (b), and Ni^{2+} (c); λ_{exc} = 300 nm.

The K_{sv} graph for Ni^{2+} is linear, indicating that the quenching event is dynamic (Fig. 3b). This can be confirmed by looking at the lifetime values for Ni^{2+}. If there is a decrease in lifetime value in the presence of the quenching reagent, the quenching is indicated to be dynamic. In the K_{sv} graph, Fe^{2+} linearity is observed in the graph at 10^{-3} M BCP. Fe^{2+} shows linearity at 10^{-4} M BCP, while at 10^{-5}M BCP, it shows positive deviation from linearity. Fe^{3+} showed a negative deviation from linearity for each concentration studied. In Fig. 3a, the Stern-Volmer plots show a negative deviation from linearity. There may exist partial accessibility of the fluorophore/heterogeneous fluorophore population.

These negative deviations suggest that the quenching event can be a combination of static and dynamic quenching, not just static quenching. The lifetime value observed in the presence of a quenching reagent will shed light on the quenching mechanism. If the lifetime value does not change in the presence of the quenching reagent, then the quenching event can be said to be static ($\tau_0/\tau = 1$) [12].

The K_{sv} values, quantum yields and R^2 values for the metals are given in Table 1. For fluorescence quantum yield (ϕ_F) calculations, 9,10-diphenyl anthracene was used as the reference material.

The fact that the quantum yield values are less than 1 indicates that the other reactions are in competition with the main reaction. Fluorescence quantum yields greater than one was obtained. This situation is indicative of chemical products being formed via photopolymerization, for instance, where one photon can lead to a cascade of chemical reactions. On the other hand, for the emission of photons, the only way to obtain quantum yields greater than one is via singlet fission. The latter is extremely rare and very hard to observe in dilute liquid samples. For one photon as the best-case scenario, the fact that the quantum yield was

greater than 1 may also be indicative of a chain reaction[Ed6]. Quantum yields larger than 1 are encountered when a mechanism exists by which one photoexcitation event can produce more than one molecule of product. Quantum yields, for example, can be very large in chain reactions, in which a single photoexcitation event initiates a repeating series of reactions leading to many molecules of product per initiation step [13]. Both the samples and the standard were excited at the same wavelength. The fluorescence was quenched in diamagnetic and paramagnetic species as well.

If the excited species contain paramagnetic ions, fluorescence may not occur with paramagnetic species due to the increased rate of transition between the systems. The presence of foreign paramagnetic ions in a fluorophore solution may have the same effect. The quenching effect of heavy metals on the fluorescence intensity of Me-β-CD can thus be explained. Many transition metal ion complexes containing partially filled *d* orbitals exhibit fluorescence in fluid solution. Many coordinated transition metal ions are paramagnetic. The low fluorescence quantum yield leads to intersystem transition of the guest molecule into a triplet within the CD cavity.

TABLE 1. Stern-Volmer (K_{sv}) Constants, *R* Squared Values (R^2) and Quantum Yields ($\phi_{FQ} - \phi_F$) in the Presence and Absence of Quenching Reagent

Heavy metal	Heavy metal concentration (M)	K_{sv}	R^2	ϕ_F	ϕ_{FQ}
Fe^{2+}	10^{-3}	89 ± 10	0.93	1.50	0.91
	10^{-4}	40 ± 5	0.91	1.41	1.10
	10^{-5}	1.4 ± 0.7	0.31	0.78	0.20
Ni^{2+}	10^{-3}	29 ± 2	0.97	1.08	0.61
	10^{-4}	43 ± 4	0.94	1.06	0.86
	10^{-5}	169 ± 24	0.89	0.87	0.27

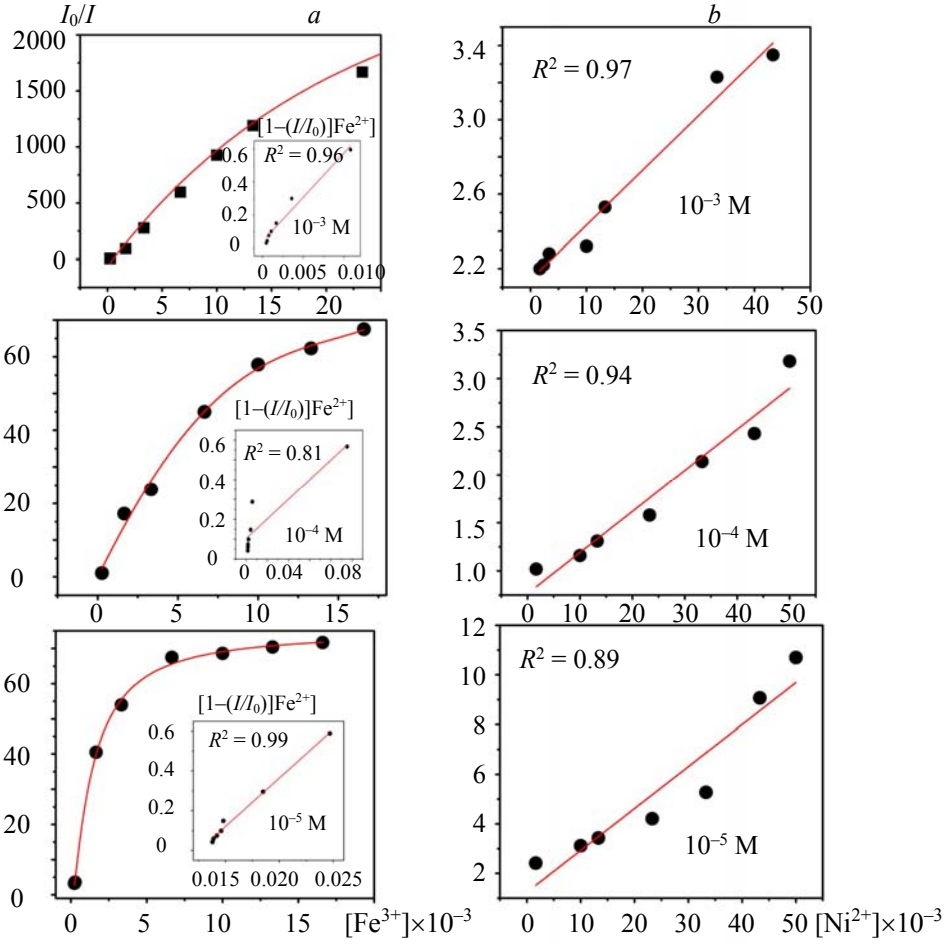

Fig. 3. Stern-Volmer plots for Fe^{3+} (a) and Ni^{2+} (b).

UV-visible spectroscopy. A PG Instrument T70+ model spectrophotometer was used for the measurement of absorption spectra. Complex formation leads to a change in the absorption spectrum of the guest molecule [14–16]. During the spectral changes, the chromophore of the guest is transferred from an aqueous medium to the nonpolar cyclodextrin. These changes must be due to a perturbation of the electronic energy levels of the guest caused either by direct interaction with the cyclodextrin, by the exclusion of solvating water molecules, or by a combination of these two effects [17, 18]. Small shifts are observed in the UV spectra of the included guests, and the method is often used to detect inclusion complexation [19–22]. Hypsochromic or bathochromic shifts or increases in absorptivity without changes in λ_{max} have been considered evidence for the interaction between cyclodextrin and bathocuproine in the formation of the complex. Figure 4 shows the absorption spectrum of bathocuproine and the inclusion complex. As described above, even the slightest shift in the UV spectrum indicates inclusion complex formation. Changes in the spectrum in Fig. 4 can be caused simply by amplification of Rayleigh scattering. Scattering by molecules with masses significantly smaller than the wavelength is called Rayleigh scattering[Ed7]. Its intensity, in contrast to the fourth force of the wavelength, depends on the size of the scattered particles and the squared measure of the particles. For the formation of Rayleigh scattering, the value of the size parameter alpha must be less than 1. Short wavelengths of visible light are more strongly affected than long wavelengths [23]. A longer wavelength shift occurs with inclusion complex formation. Some molecules are selective at scattering. They scatter short wavelengths of visible light more effectively than long wavelengths. These molecules may be effective in scattering, but the main effect here is inclusion complex formation. This is also supported by the absorption spectrum in Fig. 4.

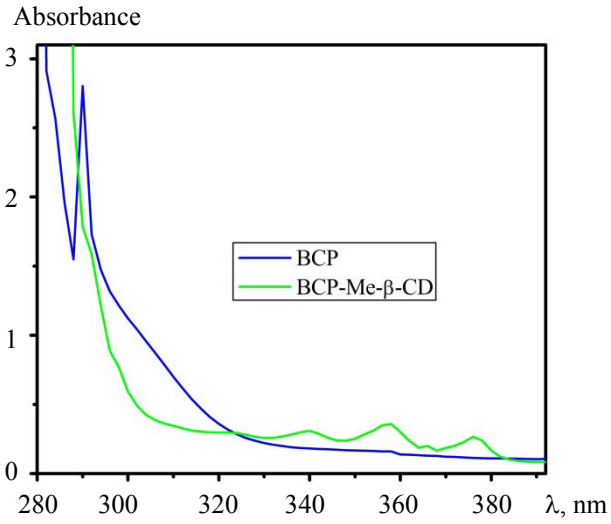

Fig. 4. Absorption spectra of bathocuproine and inclusion complexes.

Lifetime analysis. The measured lifetime value (τ_F) for BCP-Me-β-CD was 4.86 ns, whereas in the presence of Fe^{2+} and Ni^{2+}, the values (τ_{FQ}) were 0.03 and 0.07 ns, respectively. These marked reductions in lifetime value in the presence of quenching reagents indicate that the quenching event is dynamic for Fe^{2+} and Ni^{2+}. Whether the quenching mechanism was diffusion controlled was investigated by comparing the calculated bimolecular quenching rate constant values with the diffusion rate constant value, 6.6×10^9 M^{-1}/s [24]. Bimolecular quenching rate constants have been calculated for Fe^{2+} and Ni^{2+} using the fluorescence lifetime value measured in the absence of the quenching reagent [25]. It is clear from these calculations that the bimolecular quenching velocity constant values calculated for Fe^{2+} and Ni^{2+} in the concentration range of 10^{-3} to 10^{-5} M vary from 34.5 to 0.10×10^9, and these values are approximately equal to or slightly greater than the diffusion rate constant. This shows that the quenching event for Fe^{2+} and Ni^{2+} is dynamic and most likely diffusion controlled.

In the presence of Fe^{3+} as a quenching reagent, the lifetime value does not change, indicating that the event is static ($\tau_0/\tau \approx 1$). In addition, a negative deviation from linearity is observed in the S-V graphs for Fe^{3+} (Fig. 3a). Similar experimental results have been observed by other researchers [26–32]. This negative deviation is attributed to various processes, such as intersystem crossing, formation of charge transfer com-

plexes both at ground and excited states, and static and dynamic quenching [33]. For Fe^{3+} metal ions, a different quenching mechanism can be considered. To explain the quenching event here, the sphere-of-action static quenching model was applied. According to this model, instantaneous or static quenching occurs when the quenching reagent and fluorophore molecule are too close to each other or come into contact at the exact moment of excitation. This event occurs at a stimulated level of a particular W fraction. Several models have been studied to describe this static quenching event, and the S-V equation has been modified as follows [26–32]:

$$I_0/I = (1 + K_{sv}[Q])/W, \tag{3}$$

where W is given by

$$W = \exp^{(-V[Q])}, \tag{4}$$

where V is the static quenching constant that represents an active volume element surrounding the excited solute molecule.

Instantaneous (static) quenching occurs in a randomly distributed system when a quencher is located in a circle with a volume of V/N and r is the radius [$V/N' = 4\pi r^3/3$] surrounding the solution molecule at the time of excitation; W, the deviation from linearity, generally depends on the quencher concentration [Q] in S-V graphs for a quencher with a high quenching capability. So, if we revise Eq. (3),

$$[1 - (I/I_0)]/[Q] = K_{sv}(I/I_0) + (1 - W)/[Q]. \tag{5}$$

Figure 3a also shows $[1 - (I/I_0)]/[Q]$ versus I/I_0 graphs for Fe^{3+} as a quencher. The S-V quenching constant (K_{sv}) was determined according to the least square method using Eq. (5) for all cases. These values are given in Table 3 with bimolecular quenching velocity parameters calculated using the $k_q = K_{sv}/\tau$ equation.

In addition, the fluorescence lifetime value in the absence of quenching reagent is given at the bottom of the table. To support static and dynamic effects, the sphere action model was used to determine the radius (r) of the kinetic distance and the magnitude (V) of the static quenching constant. Using Eq. (5), the V and r values were determined using the least squares fit method, and these values are shown in Table 2.

TABLE 2. Quenching Parameters and Quantum Yield Values of the Inclusion Complex in the Presence of Quenching Reagent at Room Temperature

$[Fe^{3+}]$, M	$\phi_{FQ}-\phi_F$	K_{sv}, M^{-1}	k_q, M^{-1}/s	V, $mol^{-1}dm^3$	r, Å
10^{-5}		49 ± 2	10.1×10^9	0.600	6.2
10^{-4}	0.11–1.85	50 ± 1	10.3×10^9	0.110	3.5
10^{-3}		54 ± 4	11.1×10^9	0.004	1.2

N o t e. $R_\gamma = 7.01$ Å, $R_Q = 0.64$ Å, R ($R_\gamma + R_Q$) = 7.65 Å, $\tau = 4.86$ ns.

The radii of the quencher and solution molecules and the R_Q and R_γ values were determined by summing the atomic volumes of all atoms forming the molecule [34]. These values are given under Table 2. The negative deviation of the S-V graphs also suggests that dynamic and static quenching can occur simultaneously [35]. A finite sink approximation model was used to determine whether the quenching event was diffusion controlled.

Finite sink approximation model. The best know expression of the finite sink approximation model is as follows [36–39]:

$$1/k_q = (1/k_d) + (1/k_a), \tag{6}$$

where $k_d = 4\pi N'RD$, and k_a is the activation energy-controlled rate constant that defines the reaction of the pairs encountering at the R reactive distance; D is the sum of the diffusion coefficients of the quencher and solution molecules; k_q is independent of [Q] in Eq. (6). However, for effective quenching in liquids, it has been frequently observed that k_q increases with [Q]. It can be dependent both on the static quenching of the soluble molecule around [Q] and on the transient effects due to the increase in the initial concentration gradient in time, or on both [40]. If, for effective quenching, the first encounter is considered and the others are neglected, the separation distance r_0 is initially defined. The range of the diffusion region of interest for the first encounter is $R \le r \le r_0$. When Eq. (6) is modified according to this interpretation, we have

$$1/k_q = 1 - (R/r_0)/k_d + (1/k_a). \tag{7}$$

This equation becomes $k_q = k_a$ in limited reaction form, both in the case of insufficient quenching, in which case $k_a << k_d$, and in the case of quenching by pure quencher solvents. If diffusion is controlled, then Eq. (7) turns into the following equation in the case of $k_a >> k_d$:

$$k_q = k_d/(1 - R/r_0). \quad (8)$$

If the r_0 value, $2\pi N'[Q]^{1/3}$, and k_d value, $4\pi N'RD$, are placed in Eq. (7), the modified S-V equation is obtained when it is divided by the fluorescence lifetime (τ) of the solution at the time of the absence of quenching reagent [35]:

$$K_{sv}^{-1} = (K_{sv}^0)^{-1} - (2\pi N'[Q]^{1/3})/4\pi N'D\tau x[Q]^{1/3}. \quad (9)$$

The D value is calculated directly from the slope of the graph according to Eq. (9). The K_{sv}^0 value corresponds to the point with the intersection of the[Editor8] y axis when $[Q] = 0$. Then, the values of k_a and k_d are calculated to see if the quenching process is diffusion controlled. The value of K_{sv}^0 can also be written as follows:

$$K_{sv}^0 = 4\pi N'DR'\tau, \quad (10)$$

where R' is the distance parameter. It is expressed as follows:

$$R' = R[1 + 4\pi N'DR/k_a]^{-1}. \quad (11)$$

According to the model hereinabove, if the k_a value is greater than the k_d value (Eq (6), it can be said that the reaction is diffusion controlled [35] (i.e., $R' < R$). However, for $R' > R$, if the k_q values determined from Eq. (5) are greater than $4\pi N'R'D$, it can be said that bimolecular fluorescence quenching reactions are diffusion controlled.

Therefore, we need to determine K_{sv}^{-1} vs $[Q]^{1/3}$ according to Eq. (9). Here, the quencher concentration ranges from 10^{-3} to 10^{-5} M. K_{sv} is equal to $[I_0/I - 1]/[Q]$. It has been frequently observed that the quenching concentration of K_{sv} values increases with $[Q]$ for effective concentration-dependent quenching. Therefore, the K_{sv} of each quencher concentration should be determined. Here, K_{sv}^{-1} values can also be found. Figure 5 shows the $[Q]^{1/3}$ vs K_{sv}^{-1} graph. It can be seen that the graphs are linear.

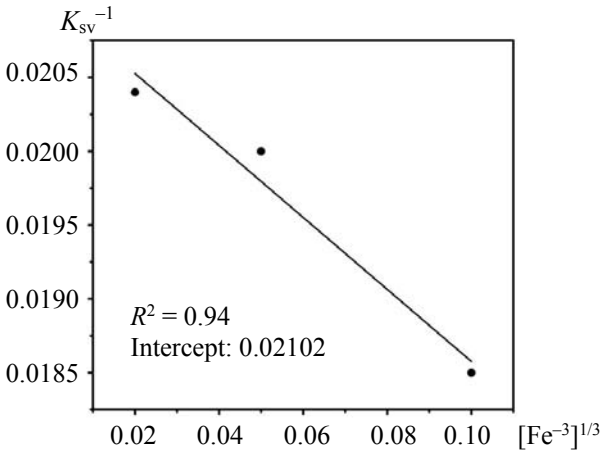

Fig. 5. K_{sv}^{-1} vs $[Q]^{1/3}$ graph for BCP-Me-β-CD.

The values of K_{sv}^0 and D are calculated from the point at which the graph intersects the[Editor9] y-axis at time $[Q] = 0$ and from the slope. Using the K_{sv}^0 and D values, R' is calculated from Eq. (9). All data for BCP-Me-β-CD at room temperature for Fe^{3+}: $[Q] = 10^{-3}$–10^{-5} M, $K_{sv}^0 = 47.6$ M^{-1}, $D = 1.74\times10^{-3}$ cm^2/s, $R' = 0.075$ Å, $4\pi N'R'D = 9.87\times10^9$ M^{-1}/s, $k_q = 9.79\times10^9$ M^{-1}/s, $k_a = 9.99\times10^9$ M^{-1}/s, $k_d = 720\times10^9$ M^{-1}/s[Ed10], $R(R_\gamma + R_Q) = 7.65$ Å.

Here, it is seen that the quenching mechanism for iron is static, as mentioned previously, since the lifetime values do not change in the presence of quenching reagent ($\tau_0/\tau \approx 1$). When $R' < R$ and the k_a value is greater than k_d according to the model, we can say that the reaction is diffusion controlled. Although $R' < R$ in our study, the k_a value is not greater than the k_d value, and thus the reaction cannot be said to be diffusion controlled. When the equation used for the finite sink approximation model (Eq. (6)) is modified only by taking into consideration the first approach with the quencher and the solution, neglecting the other ap-

proaches, according to Eq. (7), the k_a value for iron is much smaller than the k_d value, which corresponds to insufficient quenching. It is also seen that $k_q \approx k_a$. As a result, the quenching mechanism for iron is not effective, and the event is static but not diffusion controlled. Furthermore, the approximate quenching activation energy values [8] calculated for Fe^{3+} according to the sphere-of-action static quenching and finite approximation models range from 5.4 to 5.8 kJ/mol.

Conclusions. With the new probe molecule BCP-Me-β-CD, the quenching effect of Fe^{2+}, Fe^{3+}, and Ni^{2+} metal ions were investigated. The Stern–Volmer and bimolecular quenching rate constants were determined. In addition, lifetime values were measured in the presence and absence of quenching reagents. All these measurements and calculations showed that the quenching event is dynamic and approximately diffusion controlled for Ni^{2+}. On the other hand, it was shown that the quenching event is static but not effective and diffusion controlled for Fe^{3+} via lifetime measurements, a sphere-of-action static model and a finite approximation model.

Acknowledgements. We wish to thank Kocaeli University Scientific Research Coordinaton Unit (BAP) (Project No. 2017/010) and our colleagues in the Chemistry Department of Gebze Technical University for their assistance in fluorescence lifetime measurements.

REFERENCES

1. R. Balgley, M. Drees, T. Bendikov, M. Lahav, A. Facchetti, M. E. Van Der Boom, *J. Mater. Chem. C*, **4**, 4634–4639 (2016).
2. Y. Kijima, N. Asai, S. I. Tamura, *Jpn. J. Appl. Phys., Regul. Pap. Short Notes Rev. Pap.*, **38**, 5274–5277 (1999).
3. D. F. O'Brien, M. A. Baldo, M. E. Thompson, S. R. Forrest, *Appl. Phys. Lett.*, **74**, 442–444 (1999).
4. H. Tang, H. Liao, L. Zhu, *Chem. Phys. Lett.*, **381**, 605–608 (2003).
5. S. Ohno, M. Tanaka, N. Teshima, T. Sakai, *Anal. Sci.*, **20**, 171–175 (2004).
6. A. C. F. De Brito, R. S. Correa, A. A. Pinto, M. J. S. Matos, J. C. Tenorio, J. G. Taylor, T. Cazati, *J. Mol. Struct.*, **1163**, 197–204 (2018).
7. U. Ay, Z. Dogruyol, N. Arsu, *Supramol. Chem*., **26**, 66–70 (2014).
8. U. Ay, S. E. Sarli, *J. Fluoresc.*, **28**, 1371–1378 (2018).
9. A. Ray, S. Das, N. Chattopadhyay, *ACS Omega*, **4**, 15–24 (2019).
10. S. Barman, B. K. Barman, M. N. J. Roy, *Mol. Struct.*, **1155**, 503–512 (2018).
11. S. E. Sarli, U. Ay, *Inorg. Chem. Commun*., **114**, 107820 (2020).
12. H. Yang, G. Ran, J. Yan, H. Zhang, X. Hu, *Luminescence*, **33**, 349–355 (2018).
13. F. A. Carey, R. J. Sundberg, *Advanced Organic Chemistry: Structure and Mechanisms*, Plenum Press, New York and London, 469 (1995), doi: 10.1007/978-1-4615-8881-5.
14. A. H. Al-Marzouqi, I. Shehatta, B. Jobe, A. Dowaidar, *J. Pharm. Sci.*, **95**, 292–304 (2006).
15. G. S. Jadhav, P. R. Vavia, *Int. J. Pharm.*, **352**, 5–16 (2008).
16. D. D. Chow, A. H. Karara, *Int. J. Pharm.*, **28**, 95–101 (1986).
17. K. Uekama, T. Fujinaga, F. Hirayama, M. Otagiri, M. Yamasaki, *Int. J. Pharm.*, **10**, 1–15 (1982).
18. N. Rajagopalan, S. C. Chen, W.-S. Chow, *Int. J. Pharm.*, **29**, 161–168 (1986).
19. K. Uekama, S. Narisawa, F. Hirayama, M. Otagiri, *Int. J. Pharm.*, **16**, 327–338 (1983).
20. G. Smulevich, A. Feis, G. Mazzi, F. F. Vincieri, *J. Pharm. Sci.*, **77**, 523–526 (1988).
21. X. Tian-Xiang, B. D. Anderson, *Int. J. Pharm.*, **59**, 45–55 (1990).
22. R. Singh, N. Bharti, J. Madan, S. N. Hiremath, *J. Pharm. Sci. Technol.*, **2**, 171–183 (2010).
23. Slideplayer.biz.tr/slide/2790521/ (visited 17.04.2020).
24. R. A. Alberty, G. G. Hammes, *J. Phys. Chem.*, **62**, 154–159 (1958).
25. Y. Cui, G. Li, N. Zhang, X. Wang, J. Xie, L. Deng, *IEEE Trans. Magn.*, **51**, 1–4 (2015).
26. R. M. Melavanki, R. A. Kusanur, M. V. Kulakarni, J. S. Kadadevarmath, *J. Lumin.*, **128**, 573–577 (2008).
27. R. M. Melavanki, N. R. Patil, H. D. Patil, R. A. Kusanur, J. S. Kadadevaramath, *Indian J. Pure Appl. Phys.*, **49**, 748–753 (2011).
28. R. M. Melavanki, R. A. Kusanur, J. S. Kadadevaramath, M. V. Kulkarni, *J. Fluoresc.*, **20**, 1175–1180 (2010).
29. R. M. Melavanki, R. A. Kusanur, J. S. Kadadevaramath, M. V. Kulakarni, *J. Lumin.*, **129**, 1298–1303 (2009).

30. N. R. Patil, R. M. Melavanki, D. Nagaraja, H. D. Patil, F. M. Sanningannavar, S. B. Kapatakar, *J. Mol. Liq.*, **180**, 112–120 (2013).
31. N. R. Patil, R. M. Melavanki, S. B. Kapatkar, K. Chandrashekhar, H. D. Patil, S. Umapathy, *Spectrochim. Acta A: Mol. Biomol. Spectrosc.*, **79**, 1985–1991 (2011).
32. H. R. Deepa, J. Thipperudrappa, H. M. Suresh Kumar, *J. Lumin.*, **132**, 1382–1388 (2012).
33. J. S. Kadadevarmath, G. H. Malimath, R. M. Melavanki, N. R. Patil, *Spectrochim. Acta A: Mol. Biomol. Spectrosc.*, **117**, 630–634 (2014).
34. http://www.molinspiration.com/cgi-bin/properties.
35. J. S. Kadadevarmath, T. P. Giraddi, G. C. Chikkur, *J. Photosci.*, **4**, 105–112 (1997).
36. J. Keizer, *J. Phys. Chem.*, **86**, 5052–5067 (1982).
37. J. Keizer, *J. Am. Chem. Soc.*, **105**, 1494–1498 (1983).
38. J. Keizer, *J. Am. Chem. Soc.*, **107**, 5319 (1985).
39. J. Keizer, *Chem. Rev.*, **87**, 167–180 (1987).
40. H. Zeng, G. Durocher, *J. Lumin.*, **63**, 75–84 (1995).